JCTC Journal of Chemical Theory and Computation

ARTICLE

pubs.acs.org/JCTC

A Multi-Objective Approach to Force Field Optimization: Structures and Spin State Energetics of d^6 Fe(II) Complexes

Christopher M. Handley and Robert J. Deeth*

Inorganic Computational Chemistry Group, Department of Chemistry, Univ. of Warwick, Gibbet Hill Road, Coventry, CV4 7AL, Great Britain

Supporting Information

ABSTRACT: The next generation of force fields (FFs), regardless of the accuracy of the potential energy representation, will always have parameters that must be fitted in order to reproduce experimental and/or *ab initio* data accurately. Single objective methods have been used for many years to automate the obtaining of parameters, but this leads to ambiguity. The solution depends on the chosen weights and is therefore not unique. There have been few advances in solving this problem, which thus remains a major hurdle for the development of empirical FF methods. We propose a solution based on multi-objective evolutionary algorithms (MOEAs). MOEAs allow the FF to be tuned against the desired objectives and offer a powerful, efficient, and automated means to reparameterize FFs, or even discover the parameters for a new potential. Here, we illustrate the application of MOEAs by reparameterizing the ligand field molecular mechanics (LFMM) FF recently reported for modeling spin crossover in iron(II)−amine complexes (Deeth et al. *J. Am. Chem. Soc.* **2010**, *132*, 6876). We quickly recover the performance of the original parameter set and then significantly improve it to reproduce the geometries and spin state energy differences of an extended series of complexes with RMSD errors in Fe−N and N−N distances reduced from 0.06 Å to 0.03 Å and spin state energy difference RMSDs reduced from 1.5 kcal mol^{-1} to 0.2 kcal mol^{-1}. The new parameter sets highlight, and help resolve, shortcomings both in the non-LFMM FF parameters and in the interpretation of experimental data for several other Fe(II)N_6 amine complexes not used in the FF optimization.

INTRODUCTION

Molecular modeling and simulation are powerful tools for probing many biological and chemical processes. Treating systems comprising many thousands or even millions of particles has become more or less routine, yet despite the power of contemporary computers, simulations using quantum mechanical (QM) methods (e.g., density functional theory (DFT)) remain relatively scarce and restricted to picosecond time scales. Hence, the development of quantitatively accurate empirical force fields (FFs) is still a high priority.

Conventional molecular mechanics (MM) techniques have been well developed for simulating systems that consist of many light atoms.[1−4] However, introducing heavy atoms, specifically transition metals (TM), into simulations presents additional complications due to their "electronic activity". TMs typically have partially filled d orbitals and support a variety of oxidation states, either of which may significantly affect the stability and structure of a given complex.

These issues, and how to deal with them within MM simulations, including our own ligand field molecular mechanics (LFMM) approach,[5] have been proposed and reviewed.[6,7] This paper deals with the even more fundamental issue of how to derive the FF parameters in the first place.

As with all FF approaches, parametrization is critical but is often considered more of a black art than a science.[8−10] The problem is exacerbated when introducing TMs into MM simulations since the additional functions, and their attendant parameters, required to describe the metal−ligand interactions introduce additional complexity over "conventional" MM.[11] Ideally, therefore, we seek automated processes that can find the optimal LFMM parameters.

There are two problems in parameter fitting: the choice of the training data and the fitting of the parameters to these training data. Typically, most FFs are parametrized to fit *ab initio* or experimental data. The exact nature of the fit depends upon the objectives that must be minimized. Ideally, the FF should reproduce accurate relative conformational energies for the complexes, as well as accurate forces and configurations (i.e., geometries) at the minima. Most parametrization methods are automated and focus on simultaneously optimizing a number of quantities (e.g., energies, forces, Hessian matrix elements, and configurations) by minimizing a single penalty function, such as the sum of the least-squares deviation.[12−15] Other automated parametrization methods have used gradients,[11,12,16,17] neural networks,[18−21] genetic programming,[22] and genetic algorithms.[8,23−27] However, the approach used by Mostaghim et al.[23] is the only one to use a multi-objective optimization algorithm (MOOA).[28]

MOOAs promise a step change in automatic parametrization which could revolutionize the application of FF methods to increasingly complex molecular and solid-state systems. This work describes our implementation of a MOOA and its first application within the LFMM framework. To illustrate the new approach, we reanalyze the MMFF94/LFMM force field for d^6 iron(II) amine spin complexes.[29] Six-coordinate iron(II) complexes support two spin states and, given the right ligand set,

Received: August 20, 2011
Published: December 01, 2011

display spin crossover (SCO) behavior. SCO represents both a challenge for molecular modeling and a significant target for functional materials which can be used as molecular switches. We demonstrate that the MOOA approach rapidly recovers the original parameter set and locates a number of improved sets which are then applied to other Fe complexes. The improved parameters reveal outlier complexes which contain structural elements in the ligands which were not covered by the original training systems. In particular, cage complexes possess six-membered chelate rings which are forced by the ligand structure to adopt boat conformations which differ for high spin and low spin versions and require modification of some of the (non-LFMM) torsional potentials. The MOOA can then be redeployed to rapidly reoptimize the LFMM parameters and regenerate a balanced FF.

MULTI-OBJECTIVE OPTIMIZATION ALGORITHMS

Most optimization methods make use of gradient descent algorithms where the aim is to find the parameters that correspond to a minimum on an error surface. The error, or objective, which is being minimized, is often the sum of the weighted sum of squared errors for a number of properties within the training set. The weighting of the sum-of-squared errors is required for two reasons. First, we can adjust the weights so that a particular property within the training set is fitted more closely. But also the weighting must be correctly allocated so that the influence of different properties is a fair reflection of the different nature of the errors (for example the difference between bond distance errors and angle variations).

Weighting of each sum-of-property error leads to a penalty function which can be minimized. However, the final set of parameters is only valid for the weights that have been allocated in the penalty function and is the only one found when in fact there can be many parameter sets that are all valid solutions. In order for there to be no ambiguity in the weights selected, prior knowledge about the force field, and the influence of the weights on the predictive power for each of the properties, is required.

The alternative to the single objective approach is to use MOOA where a number of objectives is optimized at once. There is no one solution that is optimal; rather there are a number of solutions that are all optimal. With respect to the search space, these solutions are better than all others when all objectives are considered. Thus, this set of solutions is the *Pareto-optimal* set.[30]

As an example, we can consider the optimal design of a supercomputer that can perform many calculations but that must also be energy efficient. These objectives are competing. The computer can be more powerful, but in turn consume more power. If it consumes less power, it may well not be as powerful a computer. None of the Pareto-optimal solutions is superior to any other, but they all are superior to the (nonoptimal) solutions. MOOA allows for a search of the design space and can aid in the design-making process.

Within MOOA approaches, genetic algorithms (GAs) are the most popular, while Kriging has also been applied to the MOOAs.[31] The use of GAs within MOOA gives us the term multi-objective evolutionary algorithm (MOEA).[30,32,33] The popularity of GAs and other evolutionary algorithms (EAs) exists because they process an entire population of solutions with each generation. The EA can then be used to generate new populations of solutions, while retaining strong parameters but promoting diversity. In this way, an EA can discover many solutions that are members of the Pareto-optimal set of solutions.

Within the field of chemistry, MOOAs and MOEAs have seen some use, particularly with respect to drug discovery, as reviewed by Nicolaou et al.[28] Force field design has had only limited exposure to these new techniques.[23,34]

The main point of MOEAs is that the Pareto front of solutions dominates all other solutions found with respect to all objectives. Within the Pareto front set of solutions, each solution dominates another solution in all objectives but one. This represents the fact that there can be no improvement in one objective without loss of performance in another.

Within MOEA, we can be more precise. We wish to minimize $\vec{y}$, the objective vector.

$$\vec{y} = \vec{f}(\vec{x}) = (f_1(\vec{x}), f_2(\vec{x}), \ldots, f_m(\vec{x})) \quad (1)$$

Here, the objective vector is a function of the decision vector (parameters) $\vec{x} = (x_1, x_2, \ldots, x_n)^T$, and the decision vectors reside in the parameter search space of $S \subset \mathscr{R}^n$. The image (performance in the objectives) of the decision vectors lies within the objective space $Z = \subset \mathscr{R}^m$. Thus, the elements of Z are the objective vectors and are composed of the objective values, $\vec{f}(\vec{x}) = (f_1(\vec{x}), f_2(\vec{x}), \ldots f_m(\vec{x}))$.[23] $\mathscr{R}^n$ and $\mathscr{R}^n$ are m and n dimensional real number spaces.

A decision vector (set of parameters), x_1, *dominates* another decision vector, x_2, if x_1 is not any worse than x_2 in any objective while still outperforming x_2 in one objective.

If x_1 is not worse than x_2 in any of the objectives, though not better than x_2, then x_1 and x_2 are deemed *equivalent*. Solutions are also equivalent if they are worse in one objective or more, while being better in others.

If x_1 is not dominated by any solution then it is deemed *Pareto Optimal*. This means all members of the Pareto Optimal set are better than each other only in one objective. Members of the Pareto Optimal set in the decision space form the Pareto Optimal Front in the image space.

In this paper, the aim is to identify the Pareto Optimal sets of parameters for the LFMM force field, where we are trying to optimize two objectives (an energy error and a distance error).

Finding these Pareto Optimal sets is necessary for further generations of the EA. A GA takes a population of known solutions and uses them to create a new population of solutions. This is performed by the simple act of crossover and mutation of the bit strings that represent the decision vector. The members of the Pareto Optimal set can be used to guide the generation of further solutions by maintaining the best strengths of previous Pareto Optimal solutions. There are a number of MOEA approaches, but here we make use of nondominated sorting genetic algorithm II (NSGA-II).[35]

Ultimately, the use of MOOAs allows for an efficient exploration of parameters, removing the need for the user to have in depth prior knowledge about the target system or the potentials used. Instead, the user is simply required to choose, from a selection of Pareto Optimal solutions, the parameter set/s that best serves their needs.

METHOD

We follow the previous work of Deeth et al.[29] on iron amine complexes for the generation of the *ab initio* training data. All DFT calculations use the Amsterdam Density Functional program version 2008.01.[36] As suggested by Swart,[37] all calculations

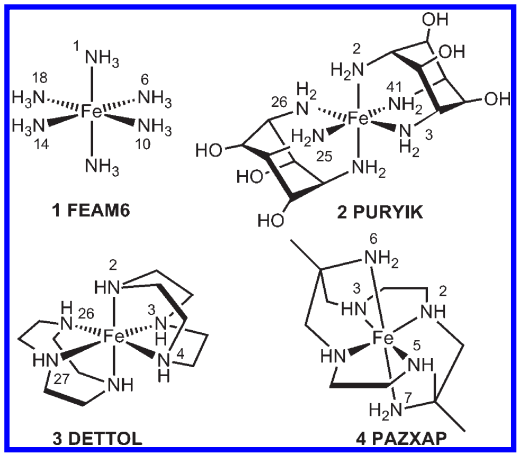

Figure 1. Schematic structures and numbering schemes for complexes used in initial LFMM FF optimization.

were performed using the OPBE functional, uncontracted triple-ζ plus polarization STO basis sets (TZP). In addition, we employ the conductor-like screening model (COSMO) to include the influence of condensed-phase effects (ε = 78, probe radius = 1.9 Å).[38] (Cartesian coordinates and ADF total binding energies for all the iron amine complexes are given in Table S1 of the Supporting Information.)

For our proof-of-principle test, we began with the original training set[29] (Figure 1). The data for this set include the optimized structures and energies for the high spin (S = 2) and low spin (S = 0) versions of four d^6 Fe(II) complexes: $[Fe(NH_3)_6]^{2+}$ (FEAM6), $[Fe(tachOH)_2]^{2+}$ (PURYIK, tachOH = 1,3,5-triamino-2,4,6-trihdyrocyclohexane[39]), $[Fe([9]aneN_3)_2]^{2+}$ (DETTOL, $[9]aneN_3$ = 1,4,7-triazacyclononane), and $[Fe(diammac)]^{2+}$ (PAZXAP, diammac = *exo*-6,13-diamino-6,13,-dimehyl-1,4,8,11-tetraazatetradecane). These complexes that span the SCO divide have been previously studied with respect to the design of potential spin crossover and light induced excited spin state trapping (LIESST) complexes.[29] Optimization and testing of the new force field parameters occurs within the DommiMOE[40] program as implemented in MOE 2010.[41] The new routine, PROTEUS (PaReto OpTimal EvolUtionary System), works with DommiMOE and optimizes the LFMM parameters for the interactions that the user has selected. We will now review the NSGA-II algorithm and detail how it has been implemented for parameter optimization.

In order to initiate parameter optimization, we first require a set of parameters. This would normally be a user's first best guess which acts as the seed from which PROTEUS explores parameter space. For LFMM, we have a number of parameters to optimize which must be varied to differing degrees. These arise from the Morse function for M−L stretches, ligand−ligand repulsion parameters which help define the angular geometry of the complexes, and angular overlap model (AOM) parameters which determine the d-orbital energies and thus the ligand field stabilization energy (LFSE).[40] Within the Morse functions, the reference distances, r_0, are varied by up to 1.5 Å in either direction, the dissociation energies, D, by up to 75% in either direction, and the α coefficients by up to 75% in either direction. Within the ligand−ligand repulsion terms, the A_{LL} parameter changes by up to 5%, while the power to which the term is raised is kept constant. The AOM parameters, e_{aom}, are derived from the $a_{aom,n}$, where aom refers to the symmetry of the M−L interaction (i.e., σ or π) and n refers to the power to which the distance between atoms is raised. In general, $e_{aom} = a_{aom,n}/r_{M-L}{}^n$. The $a_{aom,n}$ parameters were allowed to vary by up to 2000 units in either direction. For example, for our systems, $a_{\sigma 6}$ starts at a value of 41 300. This means we vary this parameter by only 0.5%. But for the electron pairing energy parameters, the variation is much larger due to the smaller magnitude of these parameters at the start of training. These limits of variation can later be reduced (or enlarged) to allow for a finer (or coarser) grade search of the local parameter space, as and when required.

Using these limits of variation of the parameters, we generate 10N sets of parameters, where N is the number of parameters that are being optimized. Each parameter set is determined randomly by generating a string of bits. Each bit is randomly determined when the string is generated. This long string of bits can then be sequentially broken up into N substrings, each of 30 bits. Later, we increase the size of these substrings to allow for a fine grade search of the local parameter space, since a longer substring length allows for smaller variations in the parameters. These substrings of bits are then decoded into real values that each lie within the limits of variation allowed for each parameter. Therefore, the initial bit string, known as a chromosome, consists of a string of zeros and ones that is NM long, where M is the length of each individual substring, in our initial case, 30.

Once each chromosome has been generated, they are decoded to give a new parameter set for which the fitness functions are evaluated. The fitness functions we use are the RMSDs between DFT and LFMM spin-state energy differences, and the RMSDs for Fe−N and N−N distances. The aim is to minimize these fitness functions.

When each parameter set has been used and the fitness functions have been evaluated for each set, the population can be sorted into Pareto fronts (following the rules outlined earlier) and assigned a rank wherein a given solution dominates all others of lower rank. The solutions are also assigned a density which describes how dense the solutions are about a particular solution. The density is the sum of distances in each of the objectives between the two nearest solutions. Using both the Pareto rank of a solution and the density, we can create new sets of parameters.

A new parameter set is created by *mating* and *mutation*. For mating, two different parameter set chromosomes are crossed over at a randomly determined point along the chromosome. This means that all bits beyond the selected chromosome now are equal to those found in the other chromosome, and vice versa. Once mating has happened, the two new *children* are mutated. Each bit in each new chromosome may be randomly changed to its opposite value.

Mating and mutation does not occur for every member of the original *parent* population. Instead, parents are selected on the basis of their Pareto rank and the density of solutions about them. For a new population of Q solutions, Q parents must be selected, as each pair of parents generates two children solutions. The parents are selected by tournament. For each parent chosen, two are randomly selected from the entire population. The rank is compared, and we retain the potential parent with the lowest rank. If the ranks are the same, then the parent with the lowest density is chosen. This method ensures elitism—i.e., the best parents should give rise to the best children—and diversity—i.e., it ensures that the parents are not too similar, which would give rise to children that do not adequately explore the parameter space.

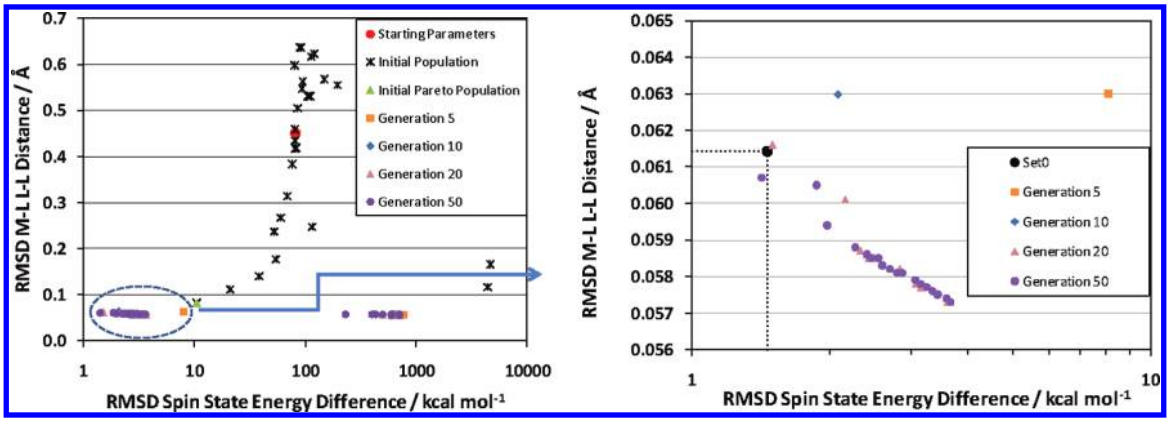

Figure 2. Left: The initial population of solutions (crosses) generated from the starting parameters (red dot on left-hand plot) is refined in round 1 of optimization to a Pareto front from which a point is selected (green triangle, the other points are not shown) to initiate round 2 of optimization: fifth generation (orange squares), 10th generation (blue diamonds), 20th generation (pink triangles), and 50th generation (purple dots). Right: Expanded view of the round 2 Pareto front solutions including the Set0 solution (black dot) from the previous study of Deeth et al.[29]).

Once all of the new solutions, the children, have been created, we have doubled the population of solutions. The children are then used, and their fitness is assessed. The entire population of both parent and children solutions is then Pareto ranked and the density for each solution found. A new population is then made that has as many members as the initial population. The population members are chosen first in order of rank. If the next set of members for the next rank is too many, such that the new population would be too large, then the members of that rank with the lowest density are selected. It is this final new population of the strongest parent and children solutions that becomes the parents to the next set of solutions. And so, the process of mating, mutation, and selection is repeated for a number of generations.

The Pareto front of the final generation of solutions is a set of equally valid solutions that can be used in simulations. Ultimately, it is up to the user to choose which parameter set to use, their choice being guided by the requirements of the problem. So if the aim of the parametrization is to provide excellent structures, while energies are not as important, then solutions can be chosen that have lower structural errors while having higher energy errors compared to other solutions.

Rather than simply run a single training session for a large number of generations, we will be training the parameters progressively. Since we have elected that the parameters can only vary by a predefined amount during each training run, there is a limit to how much we can improve the parameters, and subsequently their performance. However, by using a member of the final generation Pareto front as the new origin for a new search, we can progressively move through the full parameter space, while exploring and optimizing parameters within a smaller region at each step. There is no predetermined number of generations for which a training session should be run. In general, the more parameters being trained, the larger the population of test sets, the longer it takes to converge on the Pareto front. Of course, it is inefficient to run a training session for more generations than is required. So, as a rule, the number of generations required for convergence has to be chosen by the user, on the basis of what they have already learnt about training the parameters beforehand. Equally, the larger the bit string used for the substrings, the longer it takes to explore parameter space and so converge. However, a fine grade search can then be performed. The same is true if the window of the parameter space search is increased. Thus, all of these modifications have to be considered when determining the number of generations used.

RESULTS

Many transition metal centers can support more than one spin state. The most common examples are six-coordinate complexes of metal ions with formal d configurations spanning d^4 through to d^7 which generally display one of two magnetic states: high spin (HS), with the maximum number of unpaired electrons—4, 5, 4, and 3, respectively—or low spin (LS) with fewer unpaired electrons—2, 1, 0, and 1, respectively.

Under favorable circumstances, the HS and LS states may lie very close in energy such that an external influence, such as heat, pressure or light, causes the spin state to change. This so-called spin crossover (SCO) behavior confers a bistability which can potentially be exploited in the field of molecular electronics, data storage, and display devices.[42]

The best known SCO complexes are d^6 Fe(II) systems.[43] Fe(II) complexes can display thermal SCO where the LS $^1A_{1g}$ state is favored at low temperature but the HS $^5T_{2g}$ state becomes favored at higher temperatures due to its greater entropy. Alternatively, some complexes can be excited from their ground state to an excited metastable state of different spin (so-called light induced excited spin state trapping or LIESST). The excited state can be stable indefinitely provided the temperature is kept low enough to prevent the thermal relaxation back to the ground state.

The spin state is determined by the balance between the d−d interelectron repulsion and the ligand field stabilization energy (LFSE). The LFSE favors low spin; interelectron repulsion favors high spin. The latter is more or less constant for a particular metal ion, so the main variable that we can tune with the ligands is Δ_{oct}. Nitrogen donor ligands have the right ligand field strength with the first identified spin crossover system being $[Fe(phen)_2(NCE)_2]$ (E = S, Se).[44−46]

The complexes shown in Figure 1 span the thermal spin crossover divide, with FEAM6 and PURYIK being HS in the solid state while DETTOL and PAZXAP are low spin. Using this data set, a force field was constructed, largely manually, which captured the spin state energetics as computed by DFT.[29] This FF was then used to design new complexes with small predicted

Table 1. Comparison of the DFT and LFMM Predicted Spin Crossover Energies ΔE (kcal mol^{-1}) Using the Previous LFMM Parameters (Set_0)[29] and Parameter Sets Discovered in the Second Round of Training Round of Parameter Searching[a]

system	ΔE(DFT)	ΔE(Set_0)	ΔE(R2S4)
FEAM6	6.7	4.71	4.89
PURYIK	1.6	1.99	2.20
DETTOL	−1.5	0.56	0.44
PAZXAP	−14.4	−13.97	−15.15
RMSD		*1.46*	*1.41*
MUE		*1.22*	*1.28*

[a] Root mean square deviations (RMSDs) and the mean unsigned errors (MUEs) are included in italics.

spin state energy differences which could potentially display SCO behavior.

In the present work, the parameters are (re)optimized with respect to minimizing two objective functions—the root-mean-squared deviation (RMSD) in DFT versus LFMM spin state energy differences (kcal mol^{-1}), and the RMSD between the DFT and LFMM Fe−N and N−N distances (Å).

Our first test is to determine whether the new parametrization method can recover the existing parameter set, Set_0. Starting with the Morse function parameters—the dissociation energy, D, the reference metal−ligand distance, r_0, and the curvature parameter, α—we significantly changed the Set_0 values from 58.3 kcal/mol, 2.15 Å, and 1.318 to 108.3 kcal/mol, 3.15 Å, and 2.10, respectively, to provide a poor starting guess (red dot in Figure 2).

In round 1 of optimization, an initial population of parameter sets is generated which conforms to the variation limits described above, and their performance is evaluated. They are then progressively refined over 50 generations to give a Pareto front of solutions, one of which was selected (the green triangle in Figure 2) to initiate round 2 of optimization. Thus, we shift the window of parameter space to allow for a progressive movement from a poor region of parameter space to a better one. We now reduce the allowed amount of variation such that the Morse functions reference distances, r_0, are varied by up to 0.5 Å in either direction. The dissociation energies, D, of the functions are varied by up to 25% in either direction, while the α coefficients are varied by up to 25% in either direction. After a further 50 generations, we arrive at a new Pareto front of solutions. Table 1 compares spin state energy differences, $\Delta E = E_{LS} - E_{HS}$ from DFT (column 2) with the previously reported LFMM parameters (Set_0) and the fourth set from round 2 (R2S4). The latter has very similar RMSDs to Set_0, demonstrating that the automated MOEA procedure can quickly recover a good solution even when the optimization is started from a poor initial guess.

Table 2 compares the parameter sets we have discovered to the original parameters. The performance of the new parameters is as good as Set_0 (a more detailed comparison of the structural features is provided in the Supporting Information, Tables S2−S6); we would ideally prefer to have energy errors, on average, of less than a 1 kcal mol^{-1}. However, we find that further training using this new starting point does not lead to much further improvement. This is not surprising as this is simply the limit of performance that can be obtained varying just the Morse potential parameters.

Table 2. Comparison of the Parameter Set Values from the First Run of Parameterization and the Original Parameters, Set_0

parameter set	D_e/kcal mol^{-1}	r_0/Å	α/Å^{-1}
Set_0	58.3	2.15	1.318
R2S4	143.8	2.15	0.828

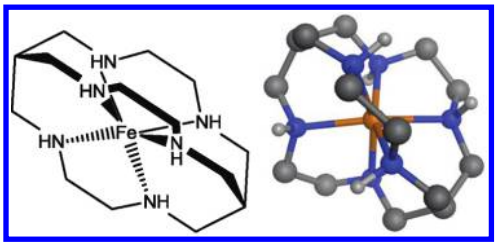

Figure 3. Structural representations of FE399.

Table 3. Comparison of the DFT and LFMM Predicted Spin State Energy Differences, Using the Original LFMM Parameters, Set_0, and Parameters Sets Obtained from Rounds 3, 4, and 5 of Optimization

system	DFT	Set_0[a]	R3S4[a]	R4S3[b]	R5S7[b]
FEAM6	6.7	4.7	3.3	4.7	6.3
PURYIK	1.6	1.4	−0.2	1.8	1.8
DETTOL	−1.5	−0.5	−2.9	−0.4	−1.4
PAZXAP	−14.4	−16.0	−18.8	−16.3	−14.5
FE399	−1.6	12.2	9.8	1.4	−1.4
RMSD		6.3	5.8	1.9	0.2
MUE		3.7	4.5	1.6	0.2

[a] Force field with original Fe−N−C−C torsion term. [b] Force field with modified Fe−N−C−C torsion.

We now apply the parameters to other iron amine complexes such as the cage species in Figure 3 (FE399), which is reported to undergo a spin transition in CD_3CN solution.[47]

However, the R2S4 parameter set (and indeed Set_0) predicts that FE399 should be strongly high spin. In contrast, DFT suggests that FE399 should be low spin by 1.6 kcal mol^{-1} and is thus consistent with potential SCO behavior. Compared to DFT, to which the LFMM parameters were tuned, the current set gives a massive energy error of nearly 14 kcal mol^{-1}. The implication is that some feature or features of FE399 are not properly covered by the systems in the training set. Consequently, we added FE399 to the original Set_0 training set and attempted to reoptimize the LFMM parameters.

The large initial error for FE399 leads to a large RMSD energy error for the whole set of 6.3 kcal mol^{-1}, but the geometrical error for FE399 is tiny. In round 3 of retraining, only the Morse function parameters were considered, but no appreciable improvement was observed (Table 3, R3S4). Extending the parameters which were varied to include ligand−ligand repulsion gave a significant improvement (Table 3, R4S3), and although the qualitative prediction for FE399 is incorrect, the DFT and LFMM ΔE values agree to within 3 kcal mol^{-1}.

We have shown that the training method can incorporate new information with little effort, and a force field can be retrained to

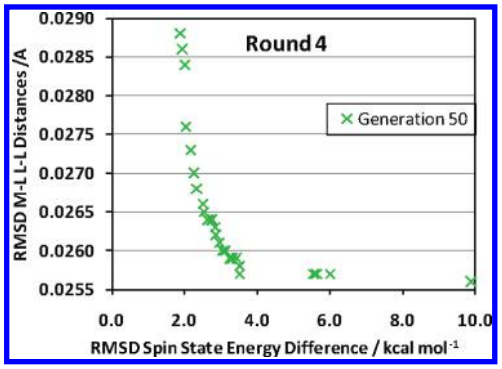

Figure 4. Final Pareto front solution from round 4 training using the extended database including FE399 but the original MMFF94 parameters.

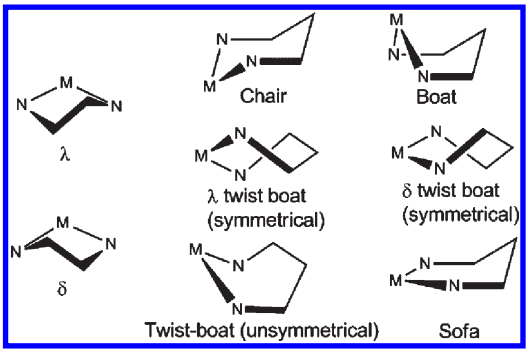

Figure 5. Conformations of five- and six-membered chelate rings.

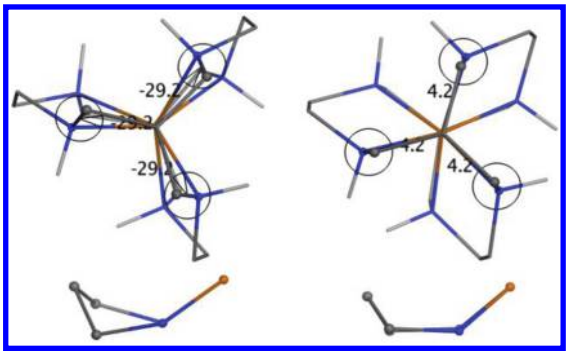

Figure 6. Detail showing the change in six-membered ring conformations going from high spin (left) to low spin (right). Nonpolar hydrogens omitted for clarity. Structures are DFT-optimized geometries.

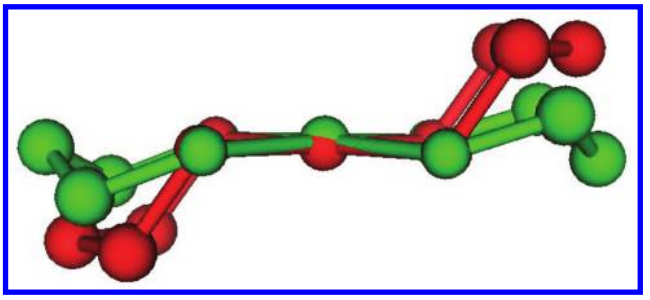

Figure 7. Calculated structure (red) of $[Cu(pn)_2]^{2+}$ without torsional constraints compared to the experimental geometry (green) from ref 48. Hydrogen atoms have been removed for clarity.

give acceptable errors. However, we were puzzled by the observation of virtually perfect agreement between the LFMM and DFT HS and LS structures of FE399 while the ΔE error was relatively large. The Pareto front of round 4 (Figure 4) suggests a limiting RMSD error in ΔE of around 2 kcal mol^{-1}. Even if we allow for *all* of the LFMM parameters to be altered, we are unable to improve much further. This suggests that there may be a problem not with the LFMM parameters but with the MMFF94 force field. It turns out that FE399 exposes an issue with the Fe−N−C−C torsion term.

The structure of the cage ligand creates two sets of six-membered chelate rings at the top and bottom of the complex connected by five-membered rings in the middle. Five-membered chelates are relatively straightforward since there are only two possibilities, δ and λ (Figure 5, left), and their torsion angles do not vary much as the metal and/or bite angle varies. In contrast, the torsion angles around six-membered rings vary dramatically with conformation.

While there are many examples of LFMM applications to both five- and six-membered chelates, FE399 possesses two unusual features. First, the six-membered rings are all obliged to adopt a boat conformation, and second, this conformation is affected by the spin state. In HS, the boat is rather twisted (the Fe−N−C−C torsion angle, τ_{boat}, is ∼29°), but the stronger ligand field for LS forces a near-perfect boat conformation with τ_{boat} equal to ∼4° (Figure 6). Thus, whereas in other complexes, the HS/LS conformations are similar and any error arising from nonideal torsional parameters cancels out, FE399 specifically highlights any shortcomings in dealing with the chair/boat conformational energy difference. Thus, our usual approach of taking a generic "reference" *−N−C−* torsional term (* represents any atom type) to describe the Fe−N−C−C torsion is found wanting.

By default, MOE assigns cos 2τ and cos 3τ terms for the Fe−N−C−C torsion which were satisfactory in the previous study but, for FE399, lead to a LS energy about 14 kcal mol^{-1} too high. We can lower the LS energy by modifying the Fe−N−C−C torsional term. By adding a cos 4τ term with a suitable force constant, the energy difference between $\tau = 30°$ and $\tau = 0°$ was reduced by about 0.5 kcal mol^{-1} (See Figure S1, Supporting Information). Given that there are six FeN_2C_3 chelate rings in FE399, this has the required effect of reducing the LS energy by the necessary amount. However, this is at the expense of a reduction in the trigonal twist of the HS complex. Of course, as per our standard procedures, the N−Fe−N−C torsional potential has zero force constants since in octahedral complexes, *trans* nitrogen donors with a bond angle of 180° would result in an undefined τ. This is not a problem for five-membered chelates, but we have already seen its effect for six-membered rings in $[Cu(pn)_2]^{2+}$ where the experimental conformation is much closer to sofa while the default MOE parameters yield a much more chairlike geometry[48] (Figure 7). This was remedied by adding explicit torsional restraints to help flatten out the pn ring. The same could have been done here except that the cage ligand constrains the rings already, plus the Fe−N−C−C torsion would need to be refined again, which seems unnecessary.

With the addition of the modified torsion term and subsequent retraining, we are able to improve the fit. In round 5, only the Morse function parameters were included, while in round 6, all LFMM parameters were reoptimized, but this did not improve

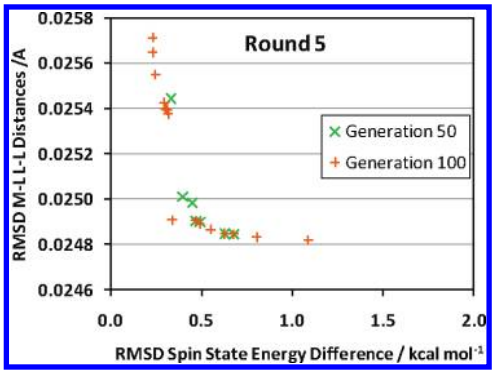

Figure 8. Pareto front from round 5 of optimization.

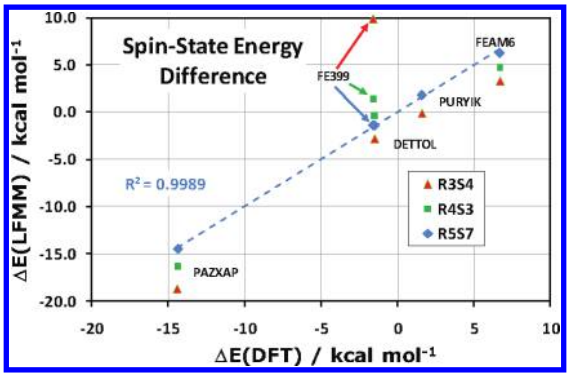

Figure 9. LFMM and DFT spin state energy difference for different parametrization scenarios: R3S4 excludes FE399 from training. R4S3 includes FE399 but retains the original MMFF94 Fe−N−C−C torsion term. R5S7 includes FE399 and the modified Fe−N−C−C torsion term.

the round 5 solutions. The final round 5 Pareto front solution is shown in Figure 8. The geometrical objective is confined to a narrow range of ∼0.001 Å, while the energy objective varies by ∼1 kcal mol^{-1}. The ΔE values for the R5S7 set are shown in Table 3.

Figure 9 compares the spin state energy differences for all five complexes (Figure 1 and FE399) for three scenarios: R3S5 excludes FE399 from training. R4S3 includes FE399 but retains the original MMFF94 Fe−N−C−C torsion term. R5S7 includes FE399 and the modified Fe−N−C−C torsion term. The latter shows that virtually perfect agreement between DFT and LFMM can be obtained using the MOEA method with the Pearson R^2 value for R5S7 of 0.9989.

Table 4 compares the LFMM parameter values for a selection of comparable round 5 solutions with the original Set$_0$. They are all broadly similar, although the MOEA sets tend to have smaller dissociation energy values and a lower Morse curvature. The a_5 term for the spin-pairing energy is also more negative.

Introducing the torsion term modification to the MMFF94 force field has had an influence on the Morse potential form, while having little effect on the ligand−ligand repulsion term, A_{LL}, and AOM parameters, e_σ and e_{ds}. What is clear from Tables 4 and 2 is that we require more data for training of the parameters, in particular for *simultaneous* fitting of D and α. The force constant that characterizes the Morse function is proportional to $D\alpha^2$. This means that for all of our parameter sets, these two

Table 4. Comparison of the LFMM Parameters from the Final Pareto Front Where All Parameters Are Being Varied

parameter	R5S7	R5S1	R5S14	Set$_0$
r_0/Å	2.186	2.190	2.191	2.15
D/kcal mol^{-1}	47.8	56.0	55.1	58.3
α	1.126	1.027	1.026	1.318
A_{LL}/kcal mol^{-1} Å^{-6}	3916	3741	3735	3935
e_σ/cm^{-1} Å^{-5}	412808	412566	413129	413000
e_{ds}/cm^{-1} Å^{-6}	125765	126125	126248	126030
a_0(pair)/kcal mol^{-1}	14.3	14.5	14.5	14.5
a_5(pair)/kcal mol^{-1} Å^{-5}	−55.5	−54.5	−55.7	−44
energy error RMSD	0.233	0.627	1.088	6.288

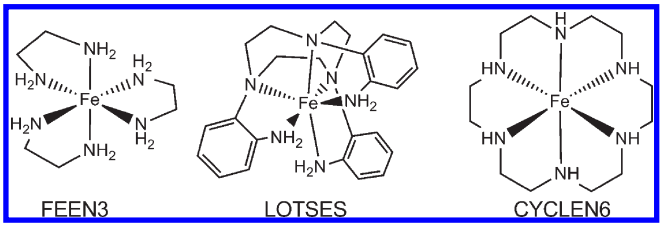

Figure 10. Structural diagrams of additional Fe(II) amine complexes.

Table 5. Calculated Spin State Energy Difference (kcal mol^{-1}) for Complexes in Figure 10

complex	ΔE(DFT)	ΔE(LFMM)[a]	$\Delta\Delta E$
FEEN3	4.7	7.0	+2.3
LOTSES	3.2	2.8	−0.4
CYCLEN6	7.2	14.7	+7.5

[a] R5S7 parameter set.

parameters can freely vary so long as this force constant remains the same, i.e., providing $D\alpha^2 \sim 60$.

Having developed an extremely accurate LFMM FF for the training set, an obvious test is to use it to model iron amine complexes which were not used in any training. Three examples were chosen—$[Fe(en)_3]^{2+}$ (FEEN3, en = ethylenediamine), [Fe(1,4,7-tris(2-aminophenyl)-1,4,7-triazacyclononane]$^{2+}$ (LOTSES), and [Fe(1,4,7,10,13,16-hexaazacyclooctadecane)]$^{2+}$ (CYCLEN6; Figure 10).

The calculated spin-state energy differences are collected in Table 5. While both theoretical methods predict that all three complexes should have high spin ground states and the detailed agreement between DFT and LFMM is satisfactory for FEEN3 and LOTSES, LFMM gives a much larger error for CYCLEN6. This correlates with the local structure around the metal center. The FeN_6 core of CYCLEN6 has the greatest deviation from octahedral symmetry, and thus the complexes used in training were not "diverse" enough to cope. This example highlights the issue of how best to choose the training data. We could include all possible systems in the training set which would give a good force field but would rapidly become unwieldy. A better solution is to develop a method which can automatically select from all possible training systems the "best"—i.e., most diverse—subset which will deliver the most accurate parameters most efficiently. This will be the subject of our next publication.

Meanwhile, we return to the systems in Figure 10 and compare the calculated results to experimental results. FEEN3 is straightforward and is reported to be a high spin complex in agreement with theory. However, for LOTSES, the single crystal X-ray diffraction structure is reported to have mean Fe−N distances of 2.10 Å and to be "predominantly low spin", the latter based on EPR and magnetometry measurements. It is difficult to reconcile the observed bond lengths with a low-spin state where distances closer to 2 Å are expected and, indeed, calculated by DFT and LFMM. Unfortunately, no details of the magnetometry experiments are provided, but we speculate that a more consistent explanation of the experimental data is that LOTSES displays a spin equilibrium in the solid state with an approximately 50/50 mix of HS and LS at room temperature. Further experimental studies could help resolve this issue.

Finally, CYCLEN6 is reported to have a temperature-dependent effective magnetic moment which has been interpreted as due to "a reversible intramolecular electron transfer"[49] between an intermediate spin (S = 1) Fe(II) species and a high spin Fe(III)−radical anion species, which becomes increasingly important as the temperature rises above 130 K. Calculations do not support this interpretation. DFT optimization of the intermediate spin (IS) state, starting from crystallographic coordinates, gives a Jahn−Teller compressed structure some 15.8 kcal mol^{-1} above the ground HS state and 8.4 kcal mol^{-1} above the LS state. While there are no doubt other possible conformations, it does not seem likely that the IS could ever become the ground state. A more plausible explanation is that the materials are not pure Fe(II) complexes. Indeed, LOTSES is also reported to have a Fe(III) impurity of ∼5%. Generating well-defined Fe(II) complexes free from paramagnetic impurities is clearly experimentally challenging.

CONCLUSIONS

We have shown that MOEAs are capable of fitting the LFMM parameters to reproduce DFT data to high accuracy with minimal energy and geometrical errors, despite starting from a parameter set which is a relatively poor guess. RMSD energy errors are reduced to just 0.2 kcal/mol with a geometrical RMSD error of 0.026 Å. Both objectives are significantly improved in a modest time (R1 training took 1 h for 30 generations, R5 took 5 h for 50 generations on a 64 bit 3 Ghz Intel Core 2 Duo laptop).

Minimizing one objective is in competition with the minimizing of the other objective. Minimizing both is ambiguous by traditional single objective methods, such as least-squares minimization, since a single parameter set is found, but this parameter set is in fact one of many, which are all equally valid and minimize the weighted sum of all errors.

MOEAs allow us to consider the payoff of optimizing one objective over another and to discover many different parameter sets which all minimize each of the objectives. The final selection of parameter sets which solve this problem is referred to as the Pareto front. All members of the Pareto front are no better than any of the other members of the Pareto front. For each pair of Pareto front solutions, both solutions will outperform the other for at least one objective. This is representative of there being no improvement in an objective without a loss of performance in another objective.

Using an implementation of MOEAs, the NSGA-II algorithm, we have not only been able to show that the method is able to recover parameters comparable to those found previously by more laborious means but have also shown that the method is able to improve substantially upon these parameters, reducing energy errors by 75% and geometry errors by 90%. Furthermore, the method was used to reparameterize the LFMM force field with respect to an expanded set of complexes, highlighting the use of this tool to easily and iteratively improve and reparameterize a force field as more and more training data become available. Most importantly, this method can allow totally new force field parameters to be discovered for systems that have never been simulated before (this being a common occurrence within LFMM) and removes this tedious and time-consuming job from the user. However, it must be remembered that this method does not overcome inherent limitations of a force field, such as missing interaction potentials, and a user is still required to recognize this need and appropriately modify the force field. A user is also required to recognize when particular parameters do not play a role in improving the objectives and so direct the training method so that it may be more efficient. In terms of effort, it can now take just a few hours to reparameterize a force field, using a modest computer where only a handful of parameters are being altered. For larger problems, it only takes a couple of days, thus allowing new potentials to be parametrized rapidly.

In summary, we have shown, using Fe−amine complexes, that MOEAs are capable and efficient machine learning methods that can parametrize force fields as well as, if not better than, a person can do manually, or by single objective methods. They are also able, unlike traditional single objective training methods, to provide a number of possible solutions, from which the user can choose the most suitable, based upon their desired performance.

ASSOCIATED CONTENT

Supporting Information. Figure S1: MMFF94 Fe−N−C−C torsion energy profiles for Fe−$NH_2CH_2CH_3$ moiety. Table S1: DFT-optimized Cartesian coordinates (Å) and ADF binding energies (kcal mol^{-1}) for complexes displayed in Figures 1, 3, and 10. Tables S2−S6: Fe−N and N−N distance comparisons for DFT and LFMM structures of FEAM6, PURYIK, DETTOL, PAZXAP (Figure 1), and FE399 (Figure 3) using the initial LFMM parameter set from ref 29. This information is available free of charge via the Internet at http://pubs.acs.org.

AUTHOR INFORMATION

Corresponding Author

*E-mail: r.j.deeth@warwick.ac.uk.

Notes

The authors declare no competing financial interest.

ACKNOWLEDGMENT

The authors acknowledge the financial support of the EPSRC for the provision of a fellowship for CMH (Grant: EP/F042159) and access to the Chemical Database Service.[50]

REFERENCES

(1) van Gunsteren, W. F.; Berendsen, H. J. C. *Groningen Molecular Simulation (GROMOS)*; University of Groningen: Groningen, The Netherlands, 1987.

(2) Brooks, B. R.; Bruccoleri, R. E.; Olafson, B. D.; States, D. J.; Swaminathan, S.; Karplus, M. *J. Comput. Chem.* **1983**, *4*, 187.
(3) Weiner, S. J.; Kollman, P. A.; Case, D. A.; Singh, U. C.; Ghio, C.; Profetajr, S.; Wiener, P. *J. Am. Chem. Soc.* **1984**, *106*, 765.
(4) Jorgensen, W. L.; Tirado-Rives, J. *J. Am. Chem. Soc.* **1988**, *110*, 1657.
(5) Deeth, R. J.; Foulis, D. L. *Phys. Chem. Chem. Phys.* **2002**, *4*, 4292.
(6) Deeth, R. J.; Anastasi, A.; Diedrich, C.; Randell, K. *Coord. Chem. Rev.* **2009**, *253*, 795.
(7) Comba, P.; Remenyi, R. *Coord. Chem. Rev.* **2003**, *238*−*239*, 9.
(8) Wang, J.; Kollman, P. A. *J. Comput. Chem.* **2001**, *22*, 1219.
(9) Bowen, J. P.; Allinger, N. In *Rev. Comput. Chem.*; Lipkowitz, K. B., Boyd, D. B., Eds.; VCH: New York, 1990; Vol. 9, p 81.
(10) Hülsmanna, M.; Müllerb, T. J.; Köddermana, T.; Reitha, D. *Mol. Simul.* **2010**, *36*, 1182.
(11) Norrby, P. O.; Liljefors, T. *J. Comput. Chem.* **1998**, *19*, 1146.
(12) Maple, J. R.; Hwang, M. J.; Stockfish, T. P.; Dinur, U.; Waldman, M.; Ewig, C. S.; Halger, A. T. *J. Comput. Chem.* **1993**, *15*, 162.
(13) Warshel, A.; Lifson, S. *J. Chem. Phys.* **1970**, *53*, 582.
(14) Halgren, T. A. *J. Comput. Chem.* **1996**, *17*, 490.
(15) Allinger, N. L.; Yuh, Y. H.; Li, J.-H. *J. Am. Chem. Soc.* **1989**, *111*, 8551.
(16) Norrby, P.-O.; Brandt, P. *Coord. Chem. Rev.* **2001**, *212*, 79.
(17) Brandt, P.; Norrby, T.; Akermark, B.; Norrby, P.-O. *Inorg. Chem.* **1998**, *37*, 4120.
(18) Marques, H. M.; Cukrowski, I. *Phys. Chem. Chem. Phys.* **2002**, *4*, 5878.
(19) Marques, H. M.; Cukrowski, I. *Phys. Chem. Chem. Phys.* **2003**, *5*, 5499.
(20) Skopec, C. E.; Robinson, J. M.; Cukrowski, I.; Marques, H. M. *J. Mol. Struct.* **2005**, *738*, 67.
(21) De Sousa, A. S.; Fernandes, M. A.; Nxumalo, W.; Balderson, J. L.; Jeftic, T.; Cukrowski, I.; Marques, H. M. *J. Mol. Struct.* **2008**, *872*, 47.
(22) Slepoy, A.; Peters, M. D.; Thompson, A. P. *J. Comput. Chem.* **2007**, *28*, 2465.
(23) Mostaghim, S.; Hoffmann, M.; Konig, P. H.; Frauenheim, T.; Teich, J. In *IEEE Congress on Evolutionary Computation (CEC 2004)*; IEEE: Portland, OR, 2004; p 212.
(24) Hunger, J.; Beyreuther, S.; Huttner, G.; Allinger, K.; Radelof, U.; Zsolnai, L. *Eur. J. Inorg. Chem.* **1998**, 693.
(25) Hunger, J.; Huttner, G. *J. Comput. Chem.* **1999**, *20*, 455.
(26) Tafipolsky, M.; Schmid, R. *J. Phys. Chem. B* **2009**, *113*, 1341.
(27) Cundari, T. R.; Fu, W. *Inorg. Chim. Acta* **2000**, *300*−*302*, 113.
(28) Nicolaou, C. A.; Brown, N.; Pattichis, C. S. *Curr. Opin. Drug Discovery Dev.* **2007**, *10*, 316.
(29) Deeth, R. J.; Anastasi, A. E.; Wilcockson, M. J. *J. Am. Chem. Soc.* **2010**, *132*, 6876.
(30) Zitzler, E.; Thiele, L. *IEEE Trans. Evol. Comp.* **1999**, *3*, 257.
(31) Hawe, G.; Sykulski, J. *COMPEL* **2008**, *27*, 836.
(32) Deb, K. In *Multiobjective Optimization*; Branke, J., Ed.; Springer-Verlag: Berlin, 2008; p 59.
(33) Burnham, C. J.; Xantheas, S. S. *J. Chem. Phys.* **2002**, *116*, 1500.
(34) Handley, C. M.; Hawe, G. I.; Kell, D. B.; Popelier, P. L. A. *Phys. Chem. Chem. Phys.* **2009**.
(35) Deb, K.; Pratrap, A.; Agrawal, S.; Meyarivan, T. *IEEE Trans. Evol. Comp.* **2002**, *6*, 182.
(36) Baerends, E. J.; Bérces, A.; Bo, C.; Boerrigter, P. M.; Cavallo, L.; Deng, L.; Dickson, R. M.; Ellis, D. E.; Fan, L.; Fischer, T. H.; Fonseca Guerra, C.; van Gisbergen, S. J. A.; Groeneveld, J. A.; Gritsenko, O. V.; Harris, F. E.; van den Hoek, P.; Jacobsen, H.; van Kessel, G.; Kootstra, F.; van Lenthe, E.; Osinga, V. P.; Philipsen, P. H. T.; Post, D.; Pye, C. C.; Ravenek, W.; Ros, P.; Schipper, P. R. T.; Schreckenbach, G.; Snijders, J. G.; Sola, M.; Swerhone, D.; te Velde, G.; Vernooijs, P.; Versluis, L.; Visser, O.; van Wezenbeek, E.; Wiesenekker, G.; Wolff, S. K.; Woo, T. K.; Ziegler, T. *ADF 2008.01*; Scientific Computing and Modelling NV, Free University, Amsterdam: Amsterdam, 2008.
(37) Swart, M. *J. Chem. Theory Comput.* **2008**, *4*, 2057.
(38) Hocking, R. K.; Deeth, R. J.; Hambley, T. W. *Inorg. Chem.* **2007**, *46*, 8238.
(39) Merbach, A. E. *Pure Appl. Chem.* **1987**, *59*, 161.
(40) Deeth, R. J.; Fey, N.; Williams-Hubbard, B. J. *J. Comput. Chem.* **2005**, *26*, 123.
(41) *MOE Molecular Operating Environment*, 2010.10; Chemical Computing Group: Montreal, Canada, 2010.
(42) Letard, J. F.; Guionneau, P.; Goux-Capes, L. In *Spin Crossover in Transition Metal Compounds III*; Guetlich, P., Goodwin, H. A., Eds.; Springer: 2004; Topics in Current Chemistry Vol. 235, p 221.
(43) Halcrow, M. A. *Polyhedron* **2007**, *26*, 3523.
(44) König, E.; Madeja, K. *Chem. Commun.* **1966**, 61.
(45) König, E.; Madeja, K. *Inorg. Chem.* **1967**, *6*, 48.
(46) Baker, W. A.; Bobonich, H. M. *Inorg. Chem.* **1964**, *3*, 1184.
(47) Martin, L. L.; Hagen, K. S.; Hauser, A.; Martin, R. L.; Sargeson, A. M. *J. Chem. Soc., Chem. Commun.* **1988**, 1313.
(48) Deeth, R. J.; Hearnshaw, L. J. A. *Dalton Trans.* **2005**, 3638.
(49) Mitewa, M.; Bontchev, P. R.; Russanov, V.; Zhecheva, E.; Mechandjiev, D.; Kabassanov, K. *Polyhedron* **1991**, *10*, 763.
(50) Fletcher, D. A.; McMeeking, R. F.; Parkin, D. *J. Chem. Inf. Comput. Sci.* **1996**, *36*, 746.